Supplementary Information (SI) for EES Catalysis.

Efficient CO_2-to-CO Conversion in Dye-Sensitized Photocatalytic Systems Enabled by Electrostatically-Driven Catalyst Binding

Vasilis Nikolaou,[a*] Palas Baran Pati,[a] Hélène Terrisse,[b*] Marc Robert,[c,d,e*] Fabrice Odobel[a*]

[a] *Nantes Université, CNRS, CEISAM, UMR 6230, F-44000 Nantes, France.*
[b] *Nantes Université, CNRS, Institut des Matériaux de Nantes Jean Rouxel, IMN, F-44000 Nantes, France.*
[c] *Université Paris Cité, CNRS, Laboratoire d'Electrochimie Moléculaire, F-75006 Paris, France.*
[d] *Sorbonne Université, CNRS, Institut Parisien de Chimie Moléculaire, F-75005 Paris, France.*
[e] *Institut Universitaire de France (IUF), F-75005, Paris, France.*

*Correspondence to: *vasileios.nikolaou@univ-nantes.fr*, *Helene.Terrisse@cnrs-imn.fr*, *robert@u-paris.fr*, and *fabrice.odobel@univ-nantes.fr*

Contents

1. Experimental section

1.1 Materials

All reagents were purchased from common commercial sources and used without any further purification, unless otherwise stated. The preparation of zinc-trimesitylporphyrin-benzoic acid (**ZnP**), and iron-tetra-(ortho-trimethylanilium)-porphyrin **Fe(*o*-TMA)** has been carried out following literature procedures.[1,2] The TiO_2 nanoparticles in this work were purchased by Sigma Aldrich: Titanium(IV) oxide – nanopowder, 21 nm primary particle size (TEM), ≥99.5% trace basis, surface area: 35-65 m^2/g .

1.2 Instrumentation

Gas Chromatography (GC): The gaseous CO_2 reduction products, (CO and H_2) were analyzed using GC analysis. Specifically, 250 µL of the reaction headspace were extracted using a gas-tight syringe and injected into an Agilent 6890N system. The GC was equipped with a CARBOPLOT P7 capillary column (25 m × 0.53 mm × 25 µm) and a thermal conductivity detector (TCD). Argon served as the carrier gas, and calibration curves were initially established for both CO and H_2. Additionally, all samples underwent testing for liquid products (formic acid, methanol, ethanol), using NMR spectroscopy; nevertheless, no additional products were detected.

Zeta potential experiments: Measurements were performed at 25°C with the Zetasizer Nano-ZS instrument from Malvern Instruments. The suspensions were introduced in the Malvern "Dip Cell" accessory, which enables zeta potential measurements in non-aqueous media. Electrophoretic mobility was determined through laser Doppler detection and then converted in a zeta potential value with the Smoluchowski model. Mean zeta potential values were obtained after four successive measurements on the same aliquot of each sample, with a delay of 30 seconds between them. The standard deviation was calculated and did not exceed 5 mV.

Infrared spectroscopy (IR): FT-IR spectrometer in ATR mode with a diamond mono-crystal was used in all our experiment. The data were processed using OPUS v8.5 and each spectrum was recorded using 32 scans.

1.3 Chemisorption of ZnP onto TiO_2 NPs.

The TiO_2 NPs were immersed in a chloroform solution containing **ZnP** (initially 0.25 µmol) and stirred at room temperature for 1 hour. Subsequently, the **ZnP-TiO_2** NPs were filtered, washed with chloroform (x3 times), dried under high vacuum, and stored under Argon in the dark. The chemisorption efficiency for **ZnP** was determined by comparing the absorption spectrum of the initial porphyrin solution (0.25 µmol) with the absorption spectrum of the supernatant solution after filtration according to the aforementioned procedure. The chemisorption percentage of **ZnP** was found to be 96%, which corresponds to 0.24 µmol/10 mg of loading (**Figure S1**).

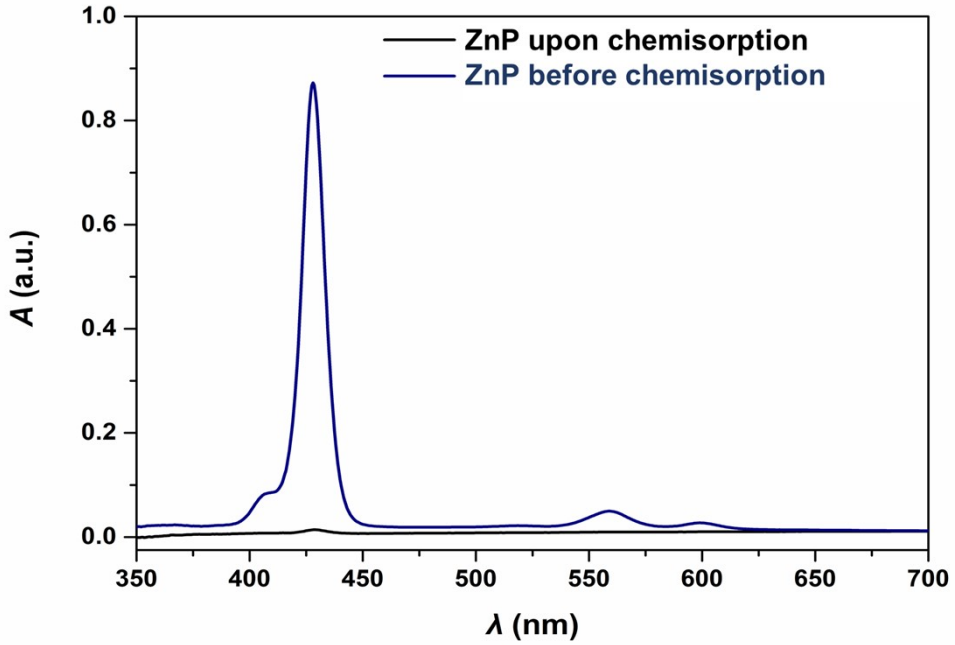

Figure S1. Absorption spectra of **ZnP** before and after chemisorption onto TiO_2 NPs.

1.4 Photocatalytic measurements

The solar-driven CO_2 reduction studies were carried out using a commercially available photobox with LED irradiation at 525 nm (10 mW/cm²).[1] Before each experiment, the dry dimethylformamide (DMF) or acetonitrile (ACN) solvent, containing 50 mM of the sacrificial electron donor (SED), namely 1,3-Dimethyl-2-phenyl-2,3-dihydro-1H-benzo[d]imidazole (BIH), was bubbled with CO_2 for 30 minutes. The photocatalytic experiments were conducted in 6.08 mL glass vials, sealed with rubber septa, at ambient pressure and temperature. **ZnP-TiO_2** NPs (0.24 or 0.12 µmol of **ZnP**), along with **Fe(*o*-TMA)** (ranging from 0.08 to 0.032 µmol) and 4mL of the SED solution, were added to the glass vials. The samples were then sonicated for 10 minutes, and then bubbled for additional 5 minutes with CO_2. Gaseous products were analyzed and quantified using gas chromatography (see section 1.2 in this SI file). In all cases, the reported CO and H_2 values, as well as the Turn Over Numbers (TONs) and the mmol/g values, represent the average of three independent experiments. Notably, the LED light source selection was based on prior research where we tested different LED irradiation sources.[1] Among 450 nm (34 mW/cm²), 6200 K cold white light (29 mW/cm²), and green LED at 525 nm (10 mW/cm²), the green LED at 525 nm achieved the highest apparent quantum efficiency (AQY) and turnover numbers (TONs).

1.5 Calculation of Turn Over Numbers (TONs) and CO evolution and apparent quantum efficiency (AQY).

- **<u>The TONs</u>** were calculated according to the following equation: **TON =** $\frac{n(CO)}{n(CAT)}$

<u>Where</u>:

***n*(CO)** is the total amount of the produced CO.

***n*(CAT)** is the total amount of **Fe(*o*-TMA)**.

- **<u>The CO evolution</u>** was calculated according to the equation:

$$\textbf{CO evolution mmol (CO)/g(cat)} = \frac{n(CO)}{m(CAT)}$$

<u>*Where*</u>:

n(CO) is the total amount of the produced CO (in mmol)

m(CAT) is the total amount of CoQPy (in grams)

- **<u>The Apparent quantum efficiency (AQY)</u>** was calculated according to the following equation:[3]

$$\textbf{AQY} = \frac{Number\ of\ electrons\ for\ CO_2\ reduction}{Number\ of\ incident\ photons} = \frac{33.2296\ \times\ \mu mol\ of\ CO\ \times\ number\ of\ e^-\ for\ CO_2\ to\ CO}{light\ intensity\ \times\ area\ \times\ time\ \times\ wavelength}$$

<u>*Where*</u>:

light intensity in mW/cm^2, area: irradiation area in cm^2, time in hours, and wavelength: irradiation wavelength in nm.

2. Infrared spectroscopy (IR)

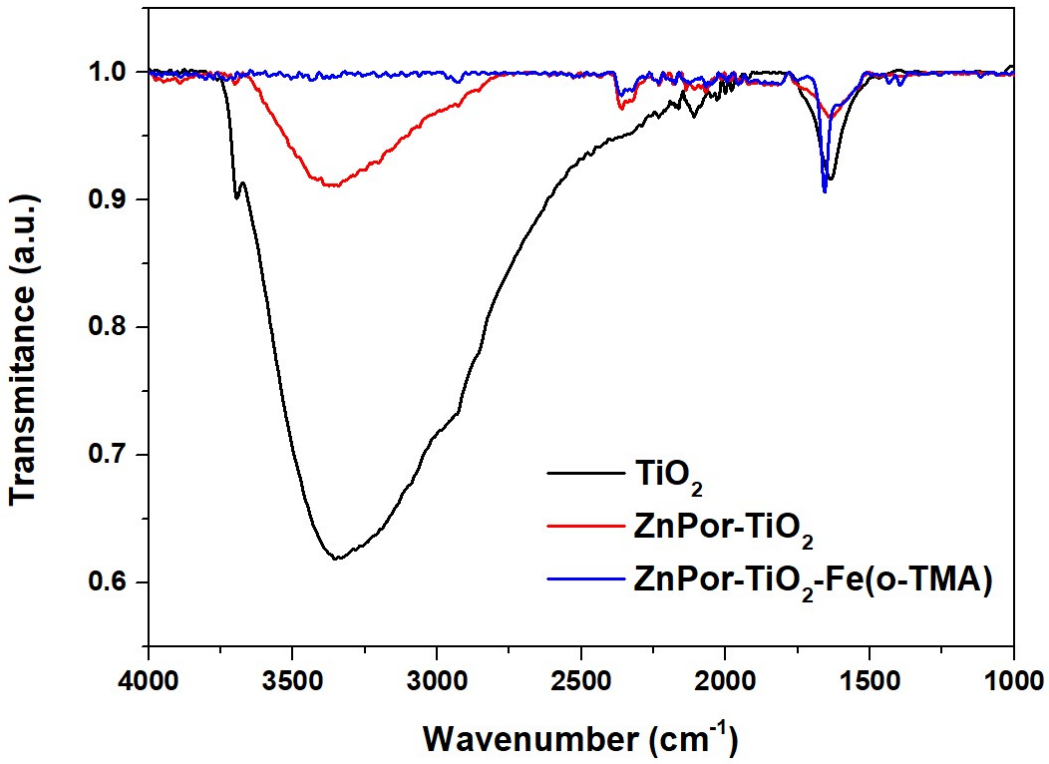

Figure S2. Infrared spectroscopy (IR) spectra TiO_2 (**black**) and ZnP@TiO_2 (**red**), and ZnP@TiO_2@Fe(o-TMA) (**blue**) at the 4000-1000 cm^{-1} region.

Description: The broad peak (at the region 3200-3600 cm^{-1}) in the IR spectrum of TiO_2 is attributed to the OH groups at the surface of TiO_2 due to O-H stretching vibrations. This peak is decreased with the addition of **ZnPor** and eliminated by the subsequent addition of **Fe-oTMA**. These FT-IR experiments demonstrate the successful functionalization of the TiO_2 particles by both the **PS** and the **CAT** and are consistent with the disappearance of free surface Ti-OH into Ti-O^-.

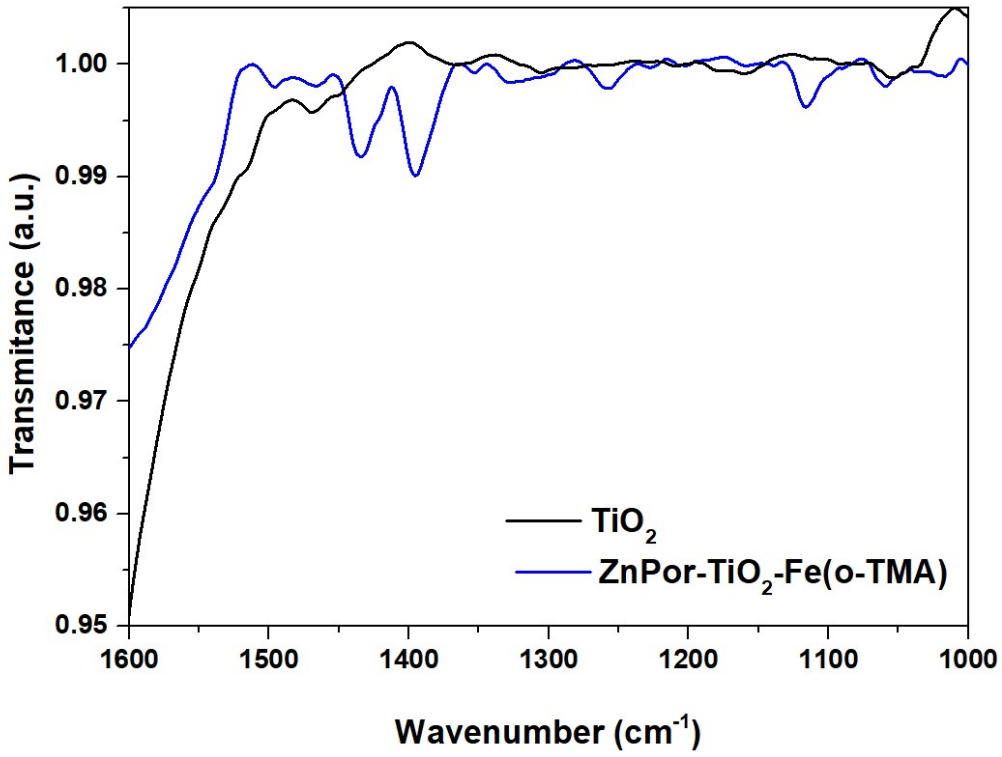

Figure S3. Infrared spectroscopy (IR) spectra TiO_2 (**black**) and ZnP@TiO_2@Fe(*o*-TMA) (**blue**) at the 1600-1000 cm^{-1} region.

Description: By comparing the IR spectrum of TiO_2 (**black line**) with ZnP@TiO_2@Fe(o-TMA) (**blue**), noticeable differencies are observed. Namely, there are no visible peaks in this area regarding TiO_2, whereas for ZnP@TiO_2@Fe(o-TMA), we detect typical peaks related to the C=C and C=N stretching of the porphyrin core (1500-1600 cm^{-1} and 1400-1300 cm^{-1}, respectively).[4]

3. Zeta potential experiments

Table S1. The different samples and conditions used for the zeta potential experiments.

Entry	Sample	Solvent	Additive	Zeta potential (mV)
1	TiO_2	DMF	-	-21 ± 2
2	ZnP@TiO_2	DMF + BIH	-	-30 ± 3
3	ZnP@TiO_2	DMF + BIH	Fe(*o*-TMA)	$+21 \pm 5$
4	TiO_2	ACN		-29 ± 5
5	ZnP@TiO_2	ACN + BIH		-39 ± 1
6	ZnP@TiO_2	ACN + BIH	Fe(*o*-TMA)	$+24 \pm 1$

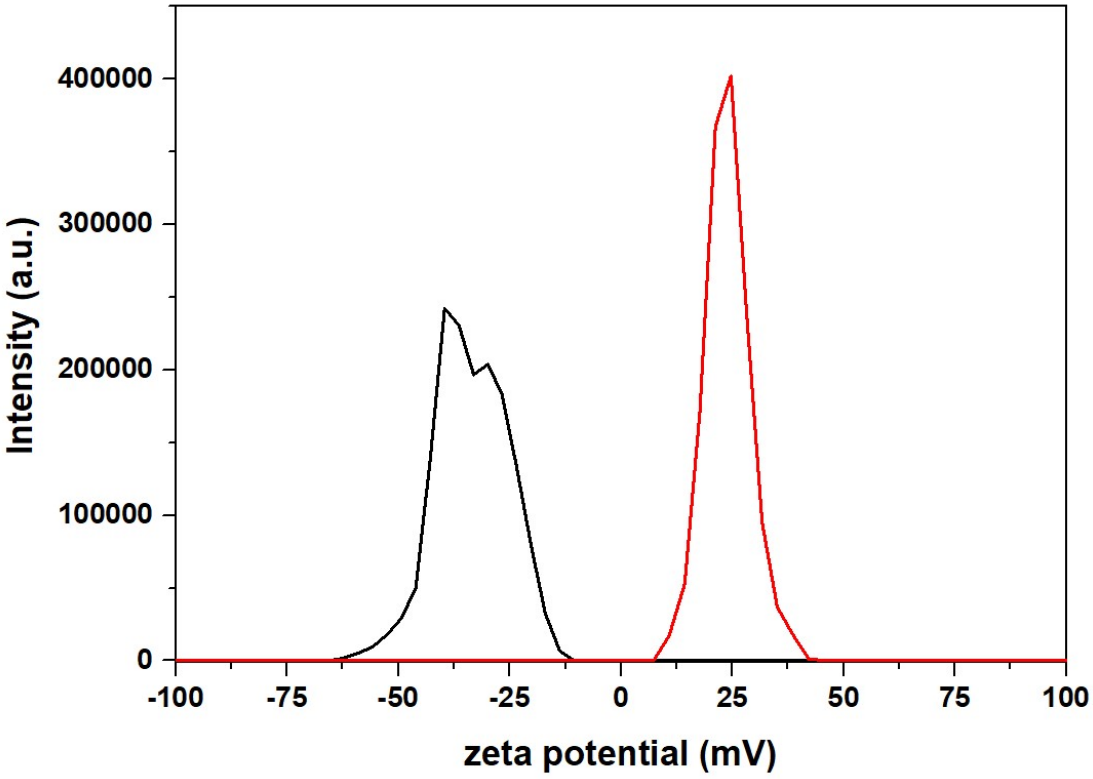

Figure S4. The zeta potential experiments of ZnP@TiO_2 (**black**), and ZnP@TiO_2 + Fe(o-TMA) (**red**) in ACN solution containing 50 mM of BIH.

4. Photocatalysis

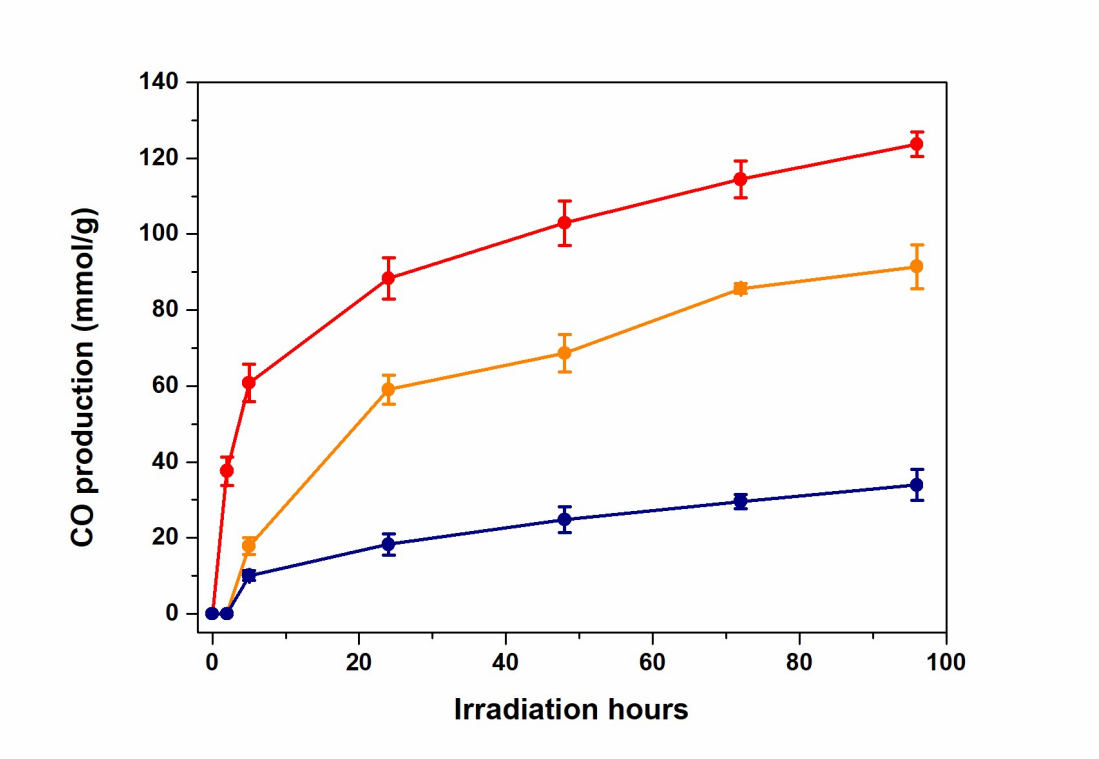

Figure S5. Photocatalytic CO_2-to-CO conversion activities of: a) ZnP (**red**), b) N_{719} (**orange**), and D_{35} (**blue**) using 0.24 µmol of PS, 0.032 µmol of Fe(*o*-TMA), in 4 mL DMF solution with 50 mM of BIH. The reported CO quantities are the average of three independently repeated experiments.

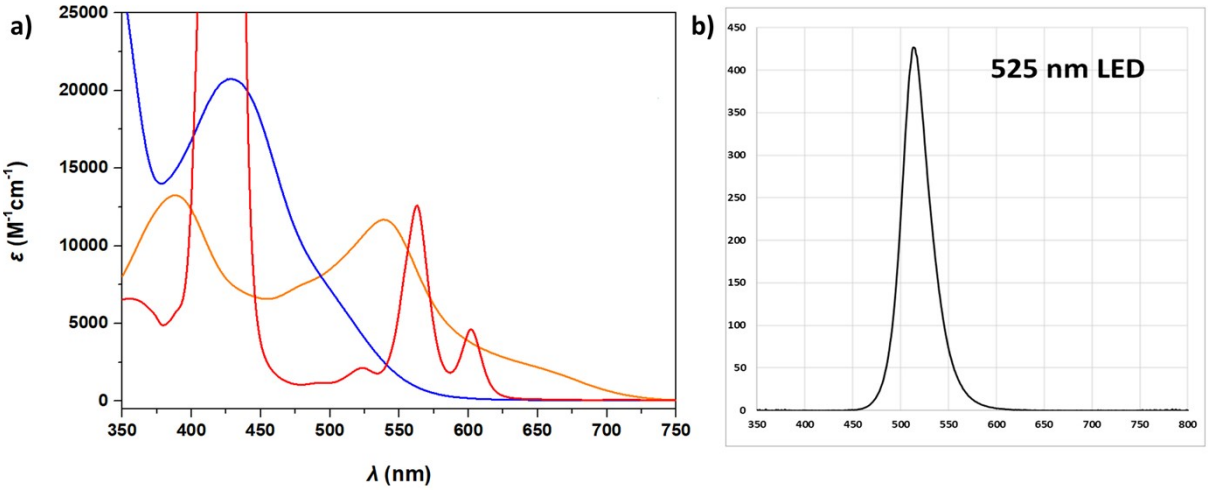

Figure S6. Absorption spectra of a): ZnP (**red**), N_{719} (**orange**), and D_{35} (**blue**) in DMF and b) the green LED-lamp used in this work.

Table S2. Electrochemical Properties of the photosensitizers (PS) used in this work. All V *vs.* SCE.

PS	Oxidation ($E_{1/2}$ox)[a]	Reduction ($E_{1/2}$red)[a]	$E_{0\text{-}0}$ [eV]	E^*_{ox} [V][b]	ΔG_{inj} [eV][c]	ΔG_{reg} [eV][d]
ZnP	0.77	-1.25	2.1	-1.33	- 0.63	-0.47
D_{35}	0.79	-1.61	2.2	-1.41	- 0.71	-0.49
N_{719}	0.70	-1.37	1.9	-1.20	- 0.50	-0.40

[a]In DMF, [b]Oxidation potential in the excited state; $E^*_{ox} = E_{1/2ox} - E_{0\text{-}0}$, [c]Driving force for electron injection into TiO_2: $\Delta G_{inj} = E^*_{ox} - E_{CB}(TiO_2)$, with $E_{CB}(TiO_2)$ = -0.7 V *vs.* SCE, [d] Driving force for the each dye regeneration by BIH ($E_{1/2ox}$ = 0.3V *vs.* SCE) $\Delta G_{reg} = E_{1/2ox}$(BIH) – E_{Ox}(dye).

Table S3. Photocatalysis results under different conditions upon 96 hours of irradiation.

Entry	ZnP	Fe(*o*-TMA)	H_2[a]	CO[a]	CO/H_2	TONs	mmol/g[b]
1	-	0.032	ND[e]	ND	-	-	-
2	0.24	-	ND	ND	-	-	-
3[c]	0.24	0.032	ND	ND	-	-	-
4[d]	0.24	0.032	ND	ND	-	-	-
5	0.24	0.032	0	6.2	**100% CO**	194	124
6	0.24	0.016	0.23	6.7	97/3	**419**	**268**
7	0.24	0.008	0.20	3.0	94/6	375	240
8	0.12	0.032	0.19	**8.0**	98/2	250	160
9	0.12	0.016	0.13	3.1	96/4	194	124

[a] in µmol; [b] mmol of CO per gram of CAT; [c] without SED; [d] without light irradiation; [e] not detected.

Note that: 0.24 µmol of ZnP corresponds to 0.2 mg of ZnP, 0.12 µmol of ZnP corresponds to 0.1 mg of ZnP, 0.032 µmol of Fe(*o*-TMA) corresponds to 0.05 mg of Fe(*o*-TMA), 0.016 µmol of Fe(*o*-TMA) corresponds to 0.025 mg of Fe(*o*-TMA), and 0.008 µmol of Fe(*o*-TMA) corresponds to 0.0125 mg of Fe(*o*-TMA).

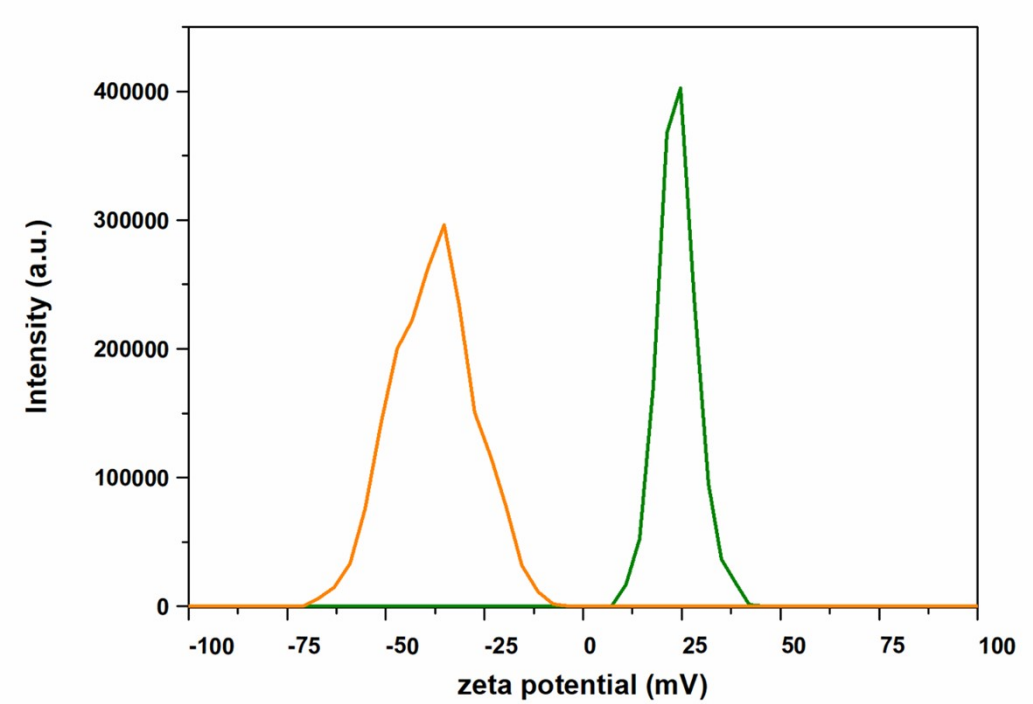

Figure S7. The zeta potential experiments of **ZnP@TiO_2 + Fe(*o*-TMA)** in ACN solution containing 50 mM of BIH, before photocatalysis (**green**) and upon photocatalysis (**orange**, 96h of irradiation).

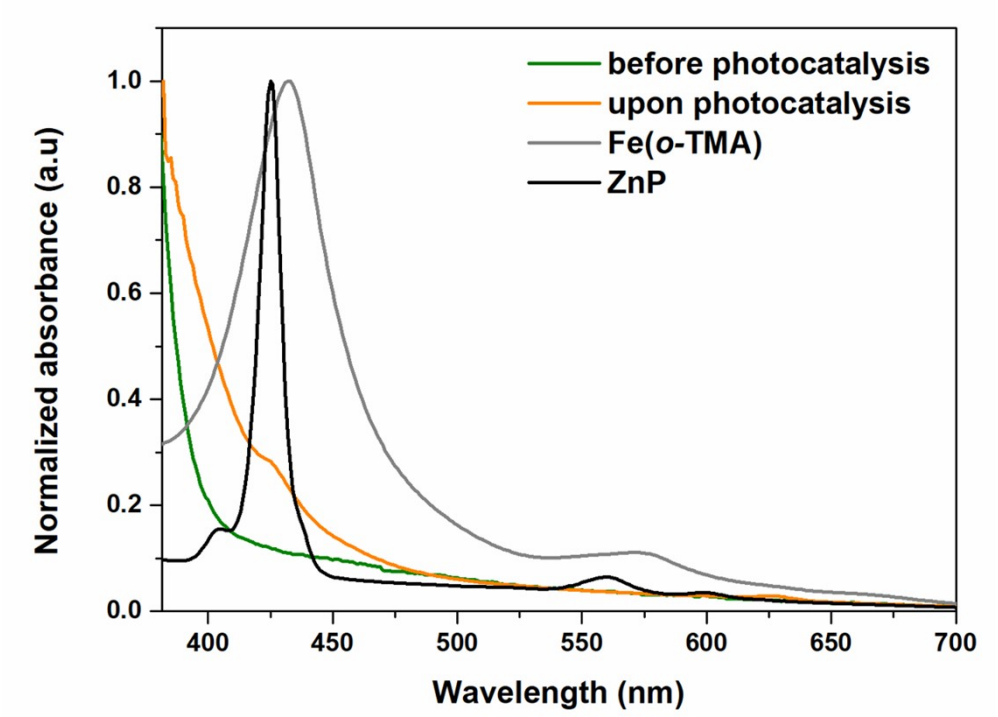

Figure S8. Absorption spectra of: **ZnP** in ACN (**black line**); **Fe(*o*-TMA)** (**gray line**) in ACN; the solution before photocatalysis (**green**, ACN containing 50 mM of BIH and 100 mM of phenol) and the solution after photocatalysis (**orange**, 96 h of irradiation).

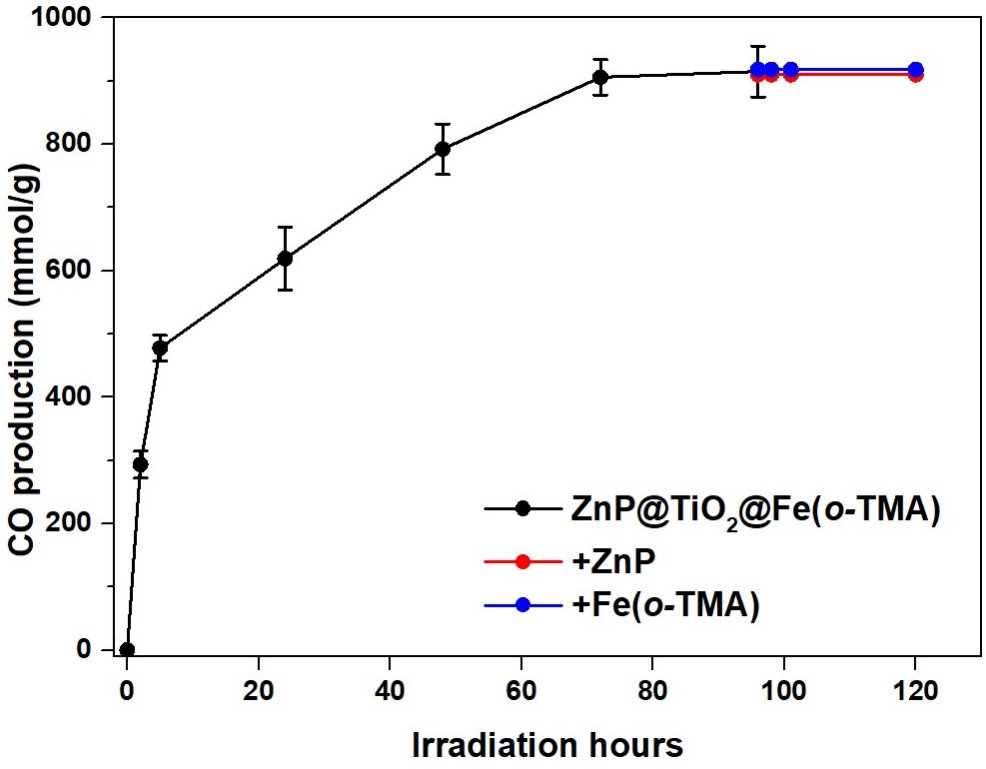

Figure S9. Stability tests of photocatalytic CO_2-to-CO conversion. Initial photocatalytic system (**black** line) contains 10mg of ZnP@TiO_2@Fe(*o*-TMA) DSPs, 4mL of ACN solution with 50mM of BIH, 0.12 µmol (0.1 mg) of ZnPor, 0.032 µmol (0.05 mg) of Fe(o-TMA) and 0.1 M of phenol. Addition of a) 0.12 µmol (0.1 mg) of ZnPor (**red**), and b) 0.032 µmol (0.05 mg) of Fe(o-TMA) (**blue**) in the reaction vial.

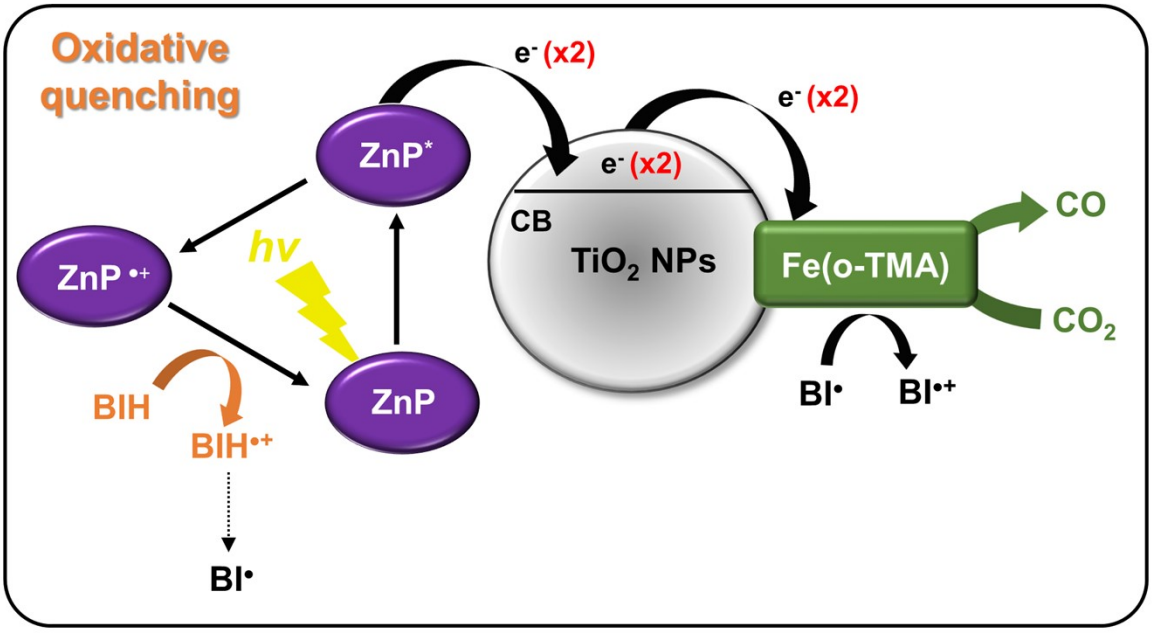

Scheme S1. Proposed photocatalytic mechanism for the two-electron reduction of CO_2 to CO in our DSPs.

Table S4. Turnover numbers (TONs), CO production rates, CO/H2 ratios, and apparent quantum yields (AQYs) of DSPs reported in the literature and in this study. In all cases, BIH was used as the sacrificial electron donor.

Entry	PS[a]	CAT[a]	TONs[b]	CO rate[c]	CO/H_2	AQY[d]	Publication
1	2-H	Re-H	922	21.2	100% CO	0.7 %	5
2	SQ_{ca}	ReC	165	3.8	~99% CO	-	6
3	ZnP_{ca}	ReC	1028	39.4	96/4	3.2 %	7
4	Dye_1	ReP	180	29.0	~99% CO	0.1 %	8
5	MOD	RePH	570	-	~99% CO	2.1 %	9
6	Dye_2	ReC	435	-	95/5	-	10
7	BDP-ZnP	CoQPy	759	42.1	66/34	-	1
8	ZnP	CoQPy	559	31.0	76/24	3.9 %	1
9[e]	**ZnP**	**Fe(*o*-TMA)**	**1658**	**95.6[f]**	**100% CO**	**16.9 %**	**this work**

[a] The molecular structures of all the different PSs and the CAT are shown in Figure S3; [b] TONs were calculated vs. CAT in all cases; [c] CO production is given in mmol g^{-1} h^{-1} (g. of CAT). The CO production rates were calculated using the given data of each publication; [d] Apparent quantum efficiency; [e] the best results are listed in this entry; [f] this CO rate (mmol g^{-1} h^{-1}) is given for 5h.

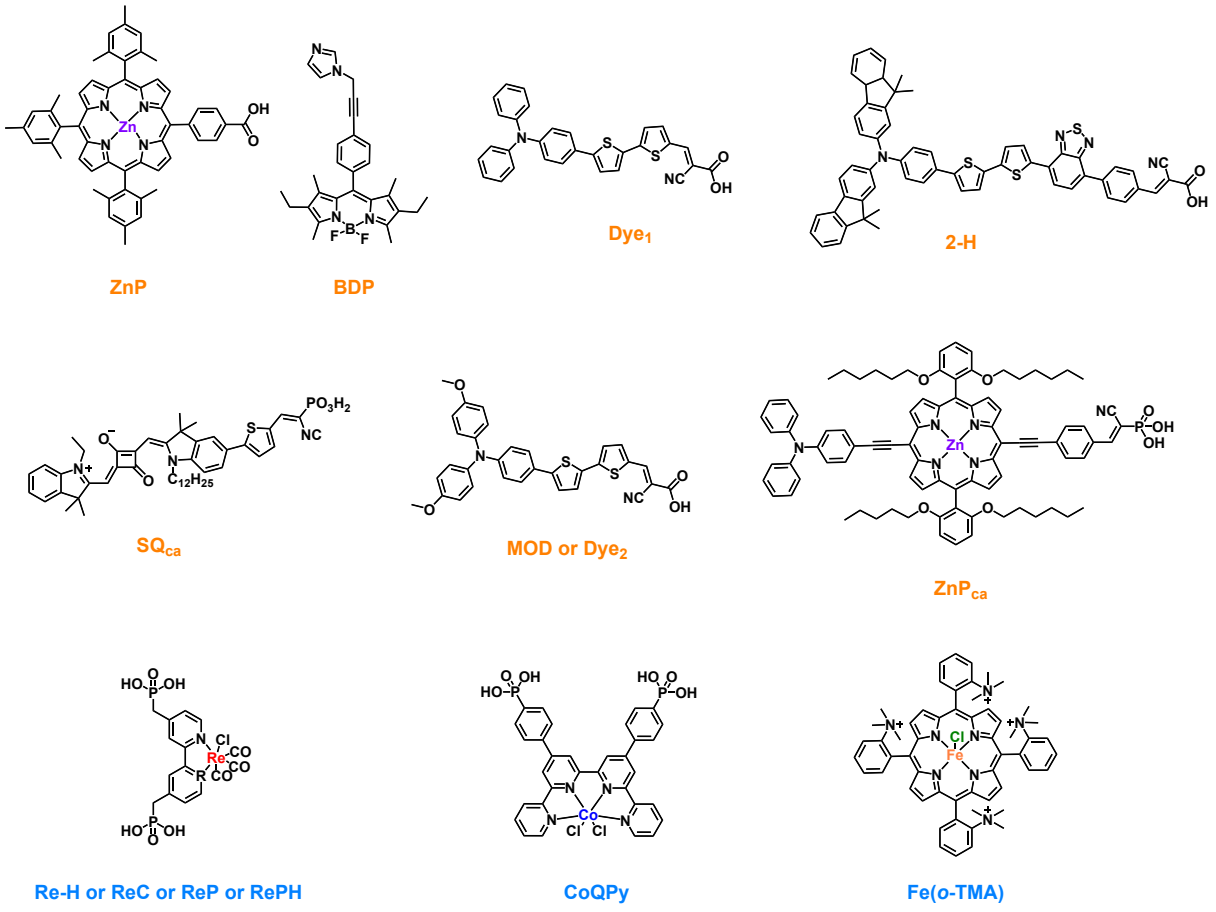

Figure S10. Molecular structures of PS (**orange**) and CAT (**blue**) listed in Table S3.

5. References

1. V. Nikolaou, et al.; *Angew. Chem. Int. Ed.* **2024**, e202318299.
2. I. Azcarate, et al.; *J. Am. Chem. Soc.* **2016**, *138*, 16639–16644.
3. S. Y. Fang, et al; *Nat. Rev. Methods Primers,* **2023**, *3*, 61.
4. Stillman, M. J., & Nicholson, R. (1989). "Spectroscopic properties of porphyrins and metalloporphyrins." The Porphyrin Handbook, Kadish, K. M., Smith, K. M., & Guilard, R. (Eds.), Academic Press.
5. S. Choi, et al.; *ACS Appl. Energy Mater*. **2022**, *5*, 10526-10541
6. M. Jo, et al.; *ACS Omega,* **2019**, *4*, 14272-14283.
7. D.-I. Won, et al.; *ACS Catal.* **2018**, *8,* 1018-1030.
8. J.-S. Lee, et al.; *Angew. Chem., Int. Ed.* **2017**, *56*, 976-980.
9. D.-I. Won, et al.; *J. Am. Chem. Soc.* **2015**, *137*, 13679-13690.
10. E.-G. Ha, et al.; *Chem. Commun.* **2014**, *50*, 4462-4464.